NANOTOXICOLOGY, 2017
VOL. 11, NO. 9-10, 1176–1194
https://doi.org/10.1080/17435390.2017.1403658

Taylor & Francis
Taylor & Francis Group

ARTICLE

Amorphous silica nanoparticles induce malignant transformation and tumorigenesis of human lung epithelial cells *via* P53 signaling

Caixia Guo[a,b], Ji Wang[a,b], Man Yang[a,b], Yang Li[a,b], Shuxiang Cui[a,b], Xianqing Zhou[a,b], Yanbo Li[a,b] and Zhiwei Sun[a,b]

[a]School of Public Health, Capital Medical University, Beijing, PR China; [b]Beijing Key Laboratory of Environmental Toxicology, Capital Medical University, Beijing, PR China

ABSTRACT

Rapid development and deployment of engineered nanomaterials, such as amorphous silica nanoparticles (SiNPs) in various commercial and biomedical applications have raised concerns about their potential adverse health effects, especially their chronic effects which have not been well addressed. In this study, human lung epithelial cells, BEAS-2B were continuously exposed to amorphous SiNPs, 5 μg/mL for 40 passages. We demonstrated here that prolonged exposure of BEAS-2B cells to amorphous SiNPs induced malignant transformation as indicated by enhanced cellular proliferation, anchorage-independent cell growth, and increased cell migration. The transformed cells induced tumorigenesis in nude mice. Furthermore, a comprehensive understanding of genome-wide transcriptional analysis was performed to clarify the molecular mechanisms based on microarray and bioinformatics analysis. Microarray data analysis demonstrated that chronic exposure of SiNPs affected expression of 821 genes, including 5 up-regulated and 816 down-regulated genes. Gene ontology and pathway analysis showed that SiNPs caused significant changes in gene expression patterns related to many important functions and pathways, mainly including response to cellular processes, oxidative stress, DNA damage, and cancer. In addition, Signal-net analysis indicated the most prominent significant role of tumor protein p53 in amorphous SiNPs-induced transformation. Further, data confirmed the inactivated p53 and aberrant p53 signaling under chronic amorphous SiNPs exposure. In summary, our data firstly demonstrated chronically low-dose amorphous SiNPs exposure resulted in malignant transformation of human lung epithelial cell *via* p53 signaling, which provides new *in vitro* evidence for the carcinogenicity of amorphous SiNPs.

ARTICLE HISTORY
Received 12 August 2016
Revised 25 September 2017
Accepted 27 October 2017

KEYWORDS
Amorphous silica nanoparticle; lung epithelial cells; cell transformation; tumorigenesis; p53

Introduction

Nanomaterials are produced in tonnage quantities in the world every year, mainly as a result of the recent advances in nanotechnologies. Silica is one of the most frequently used materials to create nanoparticles (NPs) due to its physical characteristics, particularly a very large surface-to-volume ratio. Silica nanoparticles (SiNPs), which belong to the Organization of Economic Cooperation and Development (OECD) list of interest and rank among the newly developed and most utilized nanomaterials in industrial nanotechnologies, can occur in a variety of forms: crystalline, simple amorphous, or mesoporous. Amorphous SiNPs is accepted as an FDA-approved food additive, and have been used in a wide range of industrial and biomedical applications (Napierska et al. 2010). Notwithstanding their extensive use, however, there are already numerous cytotoxicity studies about amorphous SiNPs raising concern about their toxic effects for human health: over-exposure to amorphous SiNPs has been shown to cause damage in cells, tissues, and organs *in vivo* (Napierska et al. 2010; Du et al. 2013), and *in vitro* (Sun et al. 2011; Gilardino et al. 2015; Guo et al. 2015). However, unlike their acute effects, the effects of chronic exposure to amorphous SiNPs have not been well remarked due to technical difficulties and limited experimental models. Up to now, there is no conclusive information available on the *in vitro*

CONTACT Zhiwei Sun zwsun@ccmu.edu.cn; Yanbo Li ybli@ccmu.edu.cn School of Public Health, Capital Medical University, No. 10 Xitoutiao, You An Men, Beijing, PR China

Supplemental data for this article can be accessed here.

carcinogenic potential of amorphous SiNPs under chronic settings.

The lung is a major target organ for airborne amorphous SiNPs exposure, which could accumulate in the lungs (Borak et al. 2012), and induce severe pulmonary epithelial thickening and fibrosis (Cho et al. 2007; Choi et al. 2008). In contrast to crystalline silica, which has been classified as carcinogenic to humans (Group 1) by the International Agency for Research on Cancer, IARC, amorphous silica was stated as 'not classifiable as to its carcinogenicity to humans' (Group 3) due to the lack of toxicological and epidemiological data for this material (Anon 1997; Guha, Straif, and Benbrahim-Tallaa 2011). It is noteworthy that during amorphous silica risk assessment, particle size was not necessarily taken into consideration. It has been recognized that nano-scale particles exhibit unique physicochemical properties and usually are more toxic than fine particles or bulk materials with the same chemical composition (Bakand, Hayes, and Dechsakulthorn 2012; Gatoo et al. 2014). As for their carcinogenic potential, amorphous SiNPs have been reported to induce cell apoptosis (Ahamed 2013), autophagy (Yu et al. 2014), DNA breakage (Mu et al. 2012), chromosomal damage (Park et al. 2011; Sergent, Paget, and Chevillard 2012), multinucleation (Wang et al. 2013; Yu et al. 2015b), and activation of key molecular events involved in carcinogenesis (Gehrke et al. 2013; Guo et al. 2015), e.g. mitogen-activated protein kinases (MAPKs), NF-κB, and Akt. In animals, repeated instillation of soluble, ultrafine amorphous silica (0.5 mg per rat, 30 times at intervals of 14 d with subsequent 8 or 9 months of recovery) induced a statistically significant tumor response (9.4%) in the lungs of rats (Kolling et al. 2011). All these results mentioned above indicated amorphous SiNPs had the carcinogenic potency, while their fundamental mechanisms of tumorigenesis are still unclear at present.

The *in vitro* cell transformation assays (CTAs), as alternatives to long-term animal studies, have been proved as a powerful tool for the prediction of human carcinogenicity induced by potent environmental carcinogens (Steinberg 2016). In fact, OECD has specific guidelines on 'Cell transformation assays for detection of chemical carcinogens' (Vasseur and Lasne 2012), and accumulated evidence confirmed that the cellular and molecular processes involved *in vitro* cell transformation are similar to those of *in vivo* carcinogenesis (Benigni, Bossa, and Tcheremenskaia 2013). According to the importance of the potential risk of amorphous SiNPs exposure on the respiratory system, human lung epithelial BEAS-2B cells, which exhibits similar characteristic and cellular response to carcinogens as the primary or normal lung cells, were used in our study. Furthermore, these cells have also been widely used to define conditions under which various agents and oncogenes cause neoplastic transformation (Rodrigues et al. 2009; Park et al. 2015). Especially, BEAS-2B cells have already been used as a good model to predict the carcinogenicity of nanomaterials, e.g. carbon nanotube (Wang et al. 2011), titanium dioxide (TiO_2) NPs (Vales, Rubio, and Marcos 2015), and also silver NPs (Choo et al. 2016). To mimic the carcinogenic process, a chronic exposure cell model was developed through BEAS-2B cells continuously exposed to a low dose of amorphous SiNPs in culture over a prolonged time period. Our data demonstrated that chronic amorphous SiNPs exposure induced malignant transformation *in vitro* and tumorigenicity *in vivo* upon injection of transformed cells into nude mouse. Morphological transformation has been reported to take place in Syrian Hamster Embryo (SHE) cells exposed to amorphous silica in the form of diatomaceous earths but not following exposure to pyrogenic amorphous silica (Elias et al. 2000; Fubini et al. 2001; Elias et al. 2006). But a recent study conducted by Darne et al. showed that unlike the crystalline form, the amorphous silica with the geometric mean diameter of 1.35 μm, did not induce SHE cell transformation (Darne et al. 2016). Currently, few studies have investigated the *in vitro* cell transformation potential of the nano-scale amorphous silica. Uboldi et al. reported that acute exposure (72-h) to amorphous SiNPs (100 μg/mL) did not induce cell transformation in the CTA assay on Balb/3T3 mouse fibroblasts (Uboldi et al. 2012). To our best knowledge, this study is the first report to assess *in vitro* malignant transformation potentials in BEAS-2B cells by low-dose and long-exposure of amorphous SiNPs. Interestingly, the further mechanistic study *via* the genome-wide transcriptional analysis and validation indicated a crucial role of p53 in amorphous SiNPs-induced malignant transformation processes, which could be important in lung tumorigenesis and

metastasis. Such chronic exposures can be useful to draw plausible conclusions about the potential human health risk of amorphous SiNPs exposures (Hristozov et al. 2012). Therefore, our data provide evidence for the finding on potential carcinogenicity of amorphous SiNPs, and strengthen the safety concern for amorphous SiNPs exposure.

Materials and methods

Amorphous SiNPs and characterization

Amorphous SiNPs were synthesized using the Stöber method and characterized as described in our previous study (Guo et al. 2015). Prior to the experimental use, its stock suspensions were sonicated through a sonicator (160 W, 20 kHz, 5 min; Bioruptor UDC-200, Belgium) in order to minimize particles' aggregation. Then its morphology and distribution were assessed by transmission electron microscopy, TEM (JEM2100; JEOL, Japan), and size was calculated by Image J software (NIH Image J system, Bethesda, MD). Additionally, its hydrodynamic size and zeta potential in cell culture medium, Dulbecco's Modified Eagle Medium, DMEM (Invitrogen, Carlsbad, CA) were detected with a Zetasizer (Nano ZS90; Malvern, United Kingdom). Meanwhile, purity was assessed by inductively coupled plasma atomic emission spectrometry (ICP-AES) (Agilent 720, Agilent Technologies, Santa Clara, CA). Endotoxin in amorphous SiNPs suspensions was detected by gel-clot limulus amebocyte lysate (LAL) assay.

Cell culture and treatment

BEAS-2B cells (human lung epithelial cells) were obtained from Cell Resource Center, Shanghai Institutes for Biological Sciences, PRC. Cells were cultured in DMEM medium supplemented with 10% fetal bovine serum, FBS (Invitrogen, Carlsbad, CA) at 37 °C in a 5% CO_2 humidified incubator. Amorphous SiNPs were suspended in DMEM culture medium and diluted to appropriate concentrations, and its possible toxicity on BEAS-2B was determined *via* MTT assay. Cell viability decreased remarkably along with the increased SiNPs concentration (supplementary Figure S1). Therefore, according to our pre-experiment' result and previous related studies (Gao et al. 2010; Zhao et al. 2013; Zhang et al. 2014), 5 μg/mL, no obvious toxicity to BEAS-2B cells, was chosen as the dosage of amorphous SiNPs in the following chronic exposure study. Cells were cultured in normal culture medium without SiNPs for at least two passages prior to further experiments. 1×10^6 cells were seeded into 10-cm (diameter) dishes for 24 h and maintained in DMEM with 10% FBS and 5 μg/mL SiNPs for 48 h per passage. This process was continued for about 18 weeks (40 passages). Passage-matched BEAS-2B cells without amorphous SiNPs treatment were used as control.

In addition, the total exposure volume was 10 mL in 100 mm cell culture dishes, respectively. From this, it may be calculated that an applied particle concentration of 5 μg/mL corresponds to a concentration of 0.90 μg/cm^2 on the surface of the culture dishes. The exposure dose adopted in our study was also evaluated by Multiple-path Particle Dosimetry (MPPD) software based on the real workplace exposure scenarios. The MPPD analysis was run with a clearance mechanism included, as evident in the 'baseline input settings' (see supplementary material Table S1). Most primary lung cancers are originated from bronchus epithelium (Hou et al. 2017). Meanwhile, a series of papers reported NPs deposited in tracheal-bronchial airway region (Smith, Cheng, and Yeh 2001; Zhang, Kleinstreuer, and Kim 2008). Thus the exposure relevance was assumed based on the tracheal-bronchial (TB) region. The predicted *in vivo* dose for per generation of TB region was shown in supplementary material Table S2. In considering the clearance mechanism of particles, the predicted concentration of amorphous SiNPs deposited on the surface of tracheal-bronchial epithelium was $0.05 \sim 1.41$ μg/cm^2 after an 8-h daily, 5-d per week exposure at the daily concentration of $1.0 \sim 27.6$ mg/m^3 (occupational amorphous SiNPs level reported) (Kim, Kim, and Yu 2014; Oh, Kim, and Kim 2014; Debia et al. 2016) in workplace.

Cell morphology and proliferation assay

Cell morphology was observed by optical microscope (Olympus IX81, Japan). Meanwhile, according to the manual of Wright-Giemsa Assay Reagent Kit (KeyGen Biotech, Nanjing, China), Giemsa staining was performed for a further cellular morphology investigation. Additionally, for a clear multinucleation observation, nuclei were stained by Hoechst 33258 and observed under a laser scanning confocal

microscope (LSM 710; Carl Zeiss Meditec AG, Jena, Germany) by capturing images at ×400 or ×1200 magnification. Fields were selected randomly, and the numbers of binucleated and multinucleated cells were counted to calculate the rate of total multinucleated cells. To evaluate and compare effects on cell proliferation, 5×10^3 the 40th passage Control (BEAS-P_{40}) and the 40th passage SiNPs-treated cells ($BEAS_{SiNPs}$-P_{40}) were seeded in 96-well plates with six replicates, and cell proliferation was quantified *via* MTT assay (Guo et al. 2016).

Cell cycle assessment

Cells were harvested, washed, fixed in ice-cold 70% ethanol, and frozen at −20 °C overnight. On the following day, after twice-wash with PBS, cells were resuspended in 450 μL of PBS solution containing 7.5 μM of propidium iodide (PI) and 100 μg/mL of RNase for 45 min at 37 °C in the dark. The DNA content was analyzed using a flow cytometer (Becton Dickinson, BD Biosciences, Franklin Lakes, NJ). At least 10 000 cells in each sample were collected and the population of cells in each phase of the cell cycle was determined using Cell ModiFIT software (Verity Software House, Topsham, ME).

Soft agar assay

Anchorage-independent growth on soft agar was performed in at least three independent experiments. Briefly, a base layer of 0.7% agar in culture media was poured into 12-well plates. After solidification, an equal amount of BEAS-P_{40} and $BEAS_{SiNPs}$-P_{40} were resuspended at a density of 300 cells in 1 mL of 0.35% agar after the agar cooled to a temperature below 40 °C, and were added over the agar base. Media (2 mL) was added on top of the agar per well. Media (1 mL) was added to each well every 3 d, before which 1 mL was removed each time. Four weeks later, large colonies (> 50 μm in diameter) were observed and counted using a microscope at 200 × magnification as previously described (Wang et al. 2011).

Wound healing assay

$BEAS_{SiNPs}$-P_{40} and BEAS-P_{40} cells were cultured in 10-cm (diameter) dishes, scratched using a sterile tip of 200 μL pipette, and continually cultured for 24 h after PBS washing for the removal of cell debris. Ultimately, cells were examined microscopically (Olympus IX81, Japan).

Xenograft tumorigenesis

Briefly, an equal number of cells (1×10^7) in 100 μL DMEM injected subcutaneously into the right armpit of 4-week-old male athymic BALB/c nude mice (River Laboratories, Vital River, Beijing, China), six mice per group (Akhtar et al. 2014). Mice were housed in sterilized filter-topped cages and maintained in a pathogen-free animal facility, and supplied with a normal diet and water *ad libitum* at the Laboratory Animal Center, Capital Medical University. All animal care and experimentations were approved by the Animal Experiments and Experimental Animal Welfare Committee of Capital Medical University. The mice were observed daily for 3–4 weeks. Tumor size was measured using an external caliper and volume was calculated using the formula: $(\text{length} \times \text{width}^2)/2$. Animals were euthanized, and tumors were removed if the animal's body weight dropped by more than 20% or if the tumor diameter exceeded 15 mm (Deeble et al. 2007). Therefore, mice were sacrificed at 24 d post-inoculation. Tumor weight was measured, fixed with 4% formalin, embedded in paraffin, sectioned, stained with hematoxylin and eosin (H&E), and analyzed by light microscopy.

Microarray analysis

For Affymetrix microarray profiling, total RNA was isolated using TRIzol reagent (Invitrogen, Carlsbad, CA) and purified with an RNeasy Mini Kit (Qiagen, Hilden, Germany) according to the manufacturer's protocol. The amount and quality of RNA were determined using a UV–Vis Spectrophotometer (Thermo, NanoDrop 2000, Waltham, MA) at an absorbance of 260 nm. The mRNA expression profiling was measured using Human Transcriptome Assay version 2.0 (Affymetrix GeneChip, Santa Clara, CA) with 59 302 gene-level probe sets. Microarray analysis was performed using Affymetrix Expression Console Software version 1.2.1 (Affymetrix, Santa Clara, CA). Raw data (CEL files) were normalized at the transcript level using the

robust multi-array average method (RMA workflow). The median summarization of transcript expressions was calculated. The gene-level data were then filtered to include only those probe sets that are in the 'core' metaprobe list, which represents *RefSeq* genes.

Bioinformatics analysis

For microarray data analysis, differentially expressed genes were identified, gene ontology (GO) analysis, pathway analysis and also gene signal transduction networks (Signal-Net) were established as described in our previous study (Hu et al. 2016). The differentially expressed genes were considered to be up- or down-regulated with 2-fold change and at least $p < 0.05$. Fisher's exact test was performed to select the significant GO and pathway, and the threshold of significance was considered as $p < 0.05$. Based on the GO and pathway analysis, Signal-Net derived from KEGG was established to show the core genes that played a vital role in the network. Networks are stored and presented as graphs, where nodes are mainly genes and edges represent relation types between the nodes, such as activation or phosphorylation. The degree is defined as the link number of one node with all of the other nodes. A higher degree indicated that a gene regulated or was regulated by more genes, implying a more important role in the signaling network. In addition, the properties of genes are described by Betweenness Centrality (BC) measures, reflecting the intermediary capacity of a node to modulate other interactions between nodes.

Quantitative real-time RT-PCR analysis

Total RNA was extracted using TRIzol reagent (Invitrogen, Carlsbad, CA) according to the manufacturer's protocol. The amount of RNA was measured spectrophotometrically by the absorbance at 260 nm. An aliquot of the total RNA (2 μg) was reverse-transcribed to cDNA using PrimeScript™ RT Master Mix (Takara, Japan). SYBR Premix Ex Taq™ II (Takara, Japan) was used for real-time PCR detection. The qRT-PCR reaction was monitored using the ABI PRISM 7500 Sequence DetectionSystem (Applied Biosystems, Foster City, CA) and was run with three biological repeats and three duplicated repeats. All levels were normalized to β-actin and fold induction was calculated by setting control conditions to one. The primers are listed in supplementary material Table S3.

Western blot analysis

The protein levels of p53 and its phosphorylation were determined by western blot analysis. As an internal control, GAPDH was also detected. Densitometric analysis of the western blots was performed using Image Lab™ Software (Bio-Rad version 3.0; Hercules, CA). The relative values of samples were measured by normalizing all data to the respective control samples of each experiment. The primary and secondary antibodies used were all purchased from Cell Signaling Technology, Boston, MA, with the detail as follows: anti-p-p53 (9281), anti-p53 (2527), anti-GAPDH (5174), and anti-Rabbit IgG (7074).

Statistical analysis

All statistical analysis was performed using SPSS version 16.0 software (SPSS, Chicago, IL). Data were expressed as means ± SD and Student's *t*-test was performed for comparisons between two treatment groups. Three or more treatment groups were compared by one-way analysis of variance (ANOVA) followed by the least significant difference (LSD) test. All comparisons were two-tailed and $p < 0.05$ was considered to be statistically significant. Multinucleated cell numbers and rate were analyzed through the chi-square test and regarded as frequencies.

Results

Characterization of amorphous SiNPs

As illustrated in TEM images (Figure 1(A)), the amorphous SiNPs had a near-spherical shape and well dispersed with the average diameter 57.66 ± 7.30 nm. Its hydrodynamic sizes and Zeta potentials in DMEM were approximately 106 nm and −32 mV, respectively (Figure 1(B,C)). In addition, its purity was better than 99.9% and endotoxin was not detected. Taken together, results demonstrated that amorphous SiNPs possessed favorable stability and monodispersity.

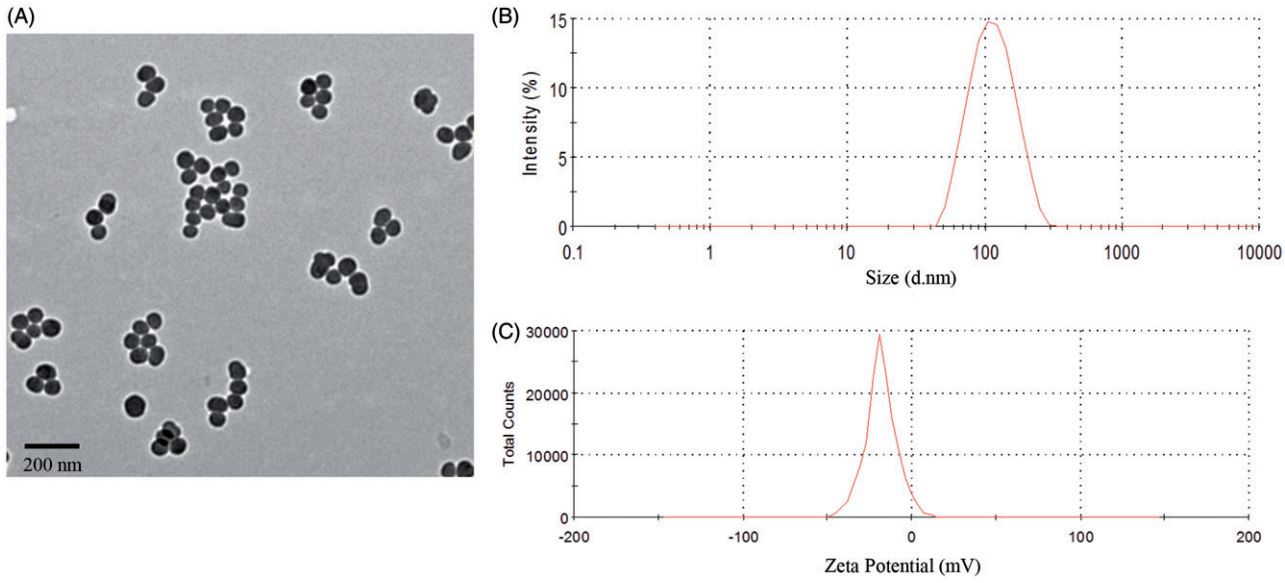

Figure 1. Characterization of amorphous SiNPs. (A) Transmission electron microscopy image. SiNPs exhibited near-spherical shape with well dispersibility. The Scale bar, 200 nm. (B) The hydrodynamic sizes and (C) zeta potential of amorphous SiNPs in DMEM media were approximately 106 nm and −32 mV, respectively.

Amorphous SiNPs induce morphological changes and alteration on cell growth patterns of human lung epithelial cells

Subconfluent cultures of BEAS-2B cells were continuously exposed to the low level of SiNPs (5 μg/mL) for 40 passages, designated as $BEAS_{SiNPs}$-P_{40}. Actually, SiNPs-treated cells exhibited morphological changes after continuously exposure for 20 passages. As shown in Figure 2(A), $BEAS_{SiNPs}$-P_{40} cells adopted a small round shape, and formed cell mounds, indicating a loss of contact inhibition which is the first indication of malignant transformation. However, the passage-matched control BEAS-2B cells, named as BEAS-P_{40}, maintained the generally more expanded and elongated shape. Giant cells containing more than one nucleus were obviously observed in $BEAS_{SiNPs}$-P_{40}, while BEAS-P_{40} were normal with round and homogeneously stained nuclei, suggesting cell multinucleation occurred upon chronic SiNPs exposure (Figure 2(B) and supplementary Figure S2). Multinucleation, an important characteristic in tumor progression and correlates to tumor grade (Couto et al. 2002), was reported after short-term NPs exposure (Huang et al. 2009; Li et al. 2011; Sycheva et al. 2011; Talebi, Khorsandi, and Moridian 2013), which may be closely associated with aberrant cytokinesis and cell fusion (Yu et al. 2015a). The quantitative analysis showed that the number of bi- and multi-nucleated cells in the $BEAS_{SiNPs}$-P_{40} cells increased significantly (6.50-fold of the BEAS-P_{40} cells) (Table 1). To determine whether chronic SiNPs exposure affects cell growth characteristic, the cellular proliferation of $BEAS_{SiNPs}$-P_{40} and BEAS-P_{40} cells were compared by MTT assay. $BEAS_{SiNPs}$-P_{40} cells showed a significant increase in cell viability above BEAS-P_{40} at 72 h post-seeding (Figure 2(C)). In addition, the quantitative analysis of cell cycle progression showed that the percentage of $BEAS_{SiNPs}$-P_{40} cells in S phase increased, while that in G_0/G_1 and G_2/M phase declined when compared to BEAS-P_{40} cells, also indicating an enhanced cell proliferation in BEAS-2B cells after chronic SiNPs exposure (Figure 2(D)).

Amorphous SiNPs induce human lung epithelial cell aggressiveness

Anchorage-independent growth of cells in soft-agar *in vitro* is one of the hallmarks of cellular transformation, with normal cells typically not capable of growth in semisolid matrices. It is closely associated with tumorigenesis *in vivo*, which is determined by measuring colony formation on soft agar (Cox and Der 1994). Significant large colonies were observed in $BEAS_{SiNPs}$-P_{40} group while no large colony in BEAS-P_{40} group, showing a characteristic of malignant cells (Figure 3(A)). Enhanced potential of migration is one of the

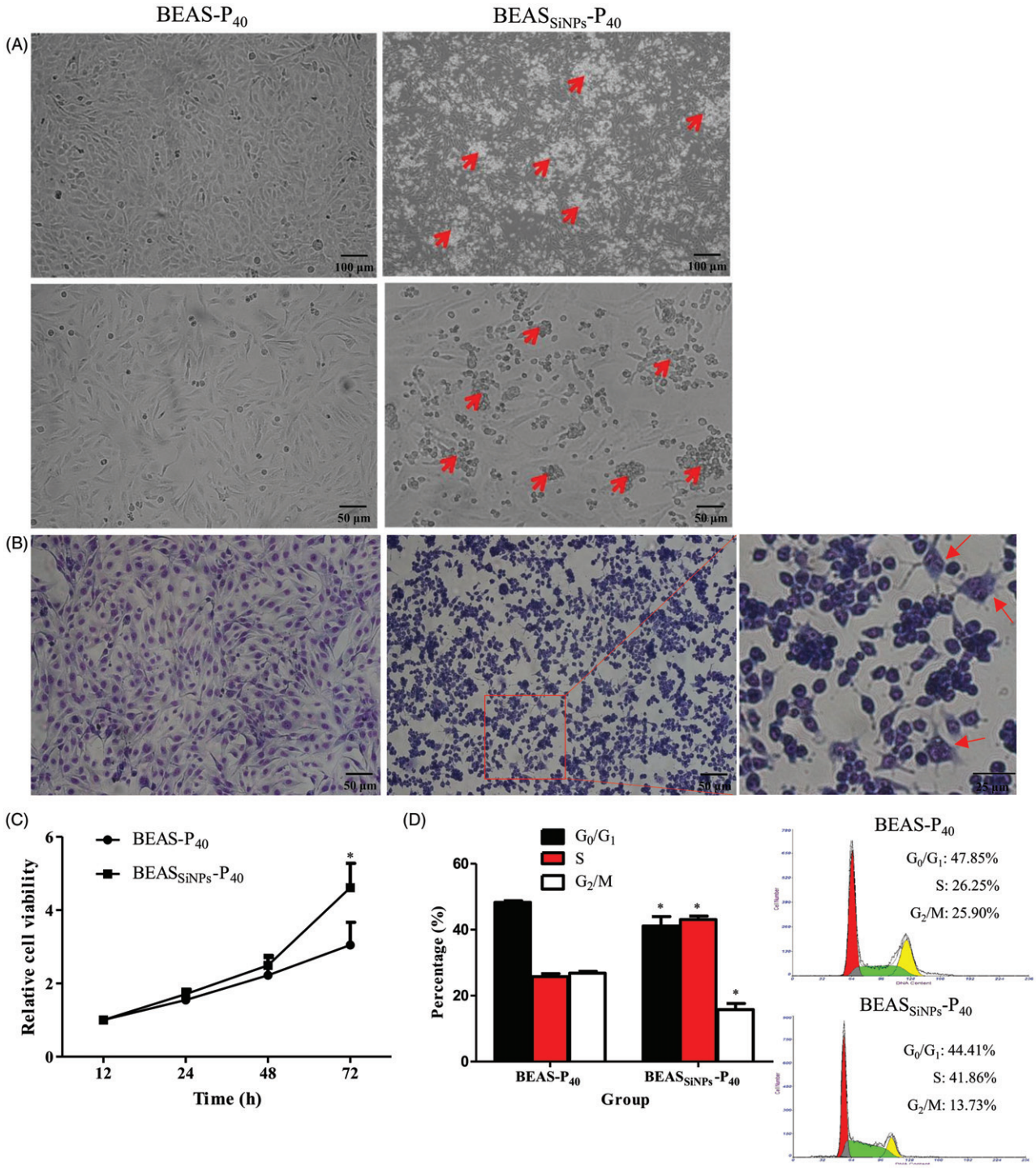

Figure 2. Amorphous SiNPs induce morphological changes and alteration on cell growth patterns of human lung epithelial cells. Subconfluent cultures (1×10^6 cells) of lung epithelial BEAS-2B cells in 10-cm (diameter) dishes were continuously exposed to 5 μg/mL amorphous SiNPs for 40 passages, 48 h for per passage. (A) Phase contrast micrographs of subconfluent monolayers of BEAS-P_{40} and $BEAS_{SiNPs}$-P_{40} cells. The red arrows indicate cell mounds. The Scale bar, 50 or 100 μm. (B) Representative images of BEAS-P_{40} and $BEAS_{SiNPs}$-P_{40} cells after Giemsa staining. The red arrows indicate multinucleated cells. The Scale bar, 50 μm. Cell proliferation curves (C) and cell cycle progressions (D) of BEAS-P_{40} and $BEAS_{SiNPs}$-P_{40} cells measured by MTT assay and FCM with PI stain, respectively. Data are means ± SD from three independent experiments. $^*p < 0.05$ vs. BEAS-P_{40}.

hallmarks of metastatic malignant cells. It has been used to assess the aggressive and malignant phenotypes of cells (Cho and Klemke 2000). As shown in Figure 3(B), the $BEAS_{SiNPs}$-P_{40} cells showed significantly enhanced migration ability than BEAS-P_{40} cells.

Amorphous SiNPs-transformed cells induce tumor formation in nude mice

Based on the stimulatory effects of amorphous SiNPs on malignant phenotypes *in vitro*, we further evaluated the tumorigenicity of SiNPs-transformed cells *in vivo* using a xenograft mouse model. At 9 d post-inoculation, palpable tumors appeared at the injection site in mice receiving $BEAS_{SiNPs}$-P_{40} cells. At 24 d post-inoculation, all six mice inoculated with $BEAS_{SiNPs}$-P_{40} cells developed large tumors mostly with the diameter over 15 mm, whereas none of the six mice inoculated with BEAS-P_{40} cells developed tumors. On the 24th d after inoculation, the $BEAS_{SiNPs}$-P_{40} tumors reached an average weight of 1.593 ± 0.696 g (Figure 4(A)). Histological inspection of tumor samples from the $BEAS_{SiNPs}$-P_{40} mice showed classic cancer cell morphology of adenocarcinoma, including allotypic epithelium, hyperchromatic nuclei, multinucleation, and also pathological karyokinesis (Figure 4(B)), strongly suggesting malignant phenotype of transformed cells. Figure 4(C) showed quantitative data for tumor volume measurements of mice inoculated with $BEAS_{SiNPs}$-P_{40} cells. These results firstly demonstrated the *in vivo*

Table 1. Number of bi- and multi-nucleated cells induced by chronic amorphous SiNPs exposure.

Group	Cell count (*n*)	Bi- and multi-nucleated cells (*n*)	Rate of bi- and multi-nucleated cells (%)
BEAS-P_{40}	500	4	0.80
$BEAS_{SiNPs}$-P_{40}	500	26	5.20*

*$p < 0.05$ vs. BEAS-P_{40} using chi-square test.

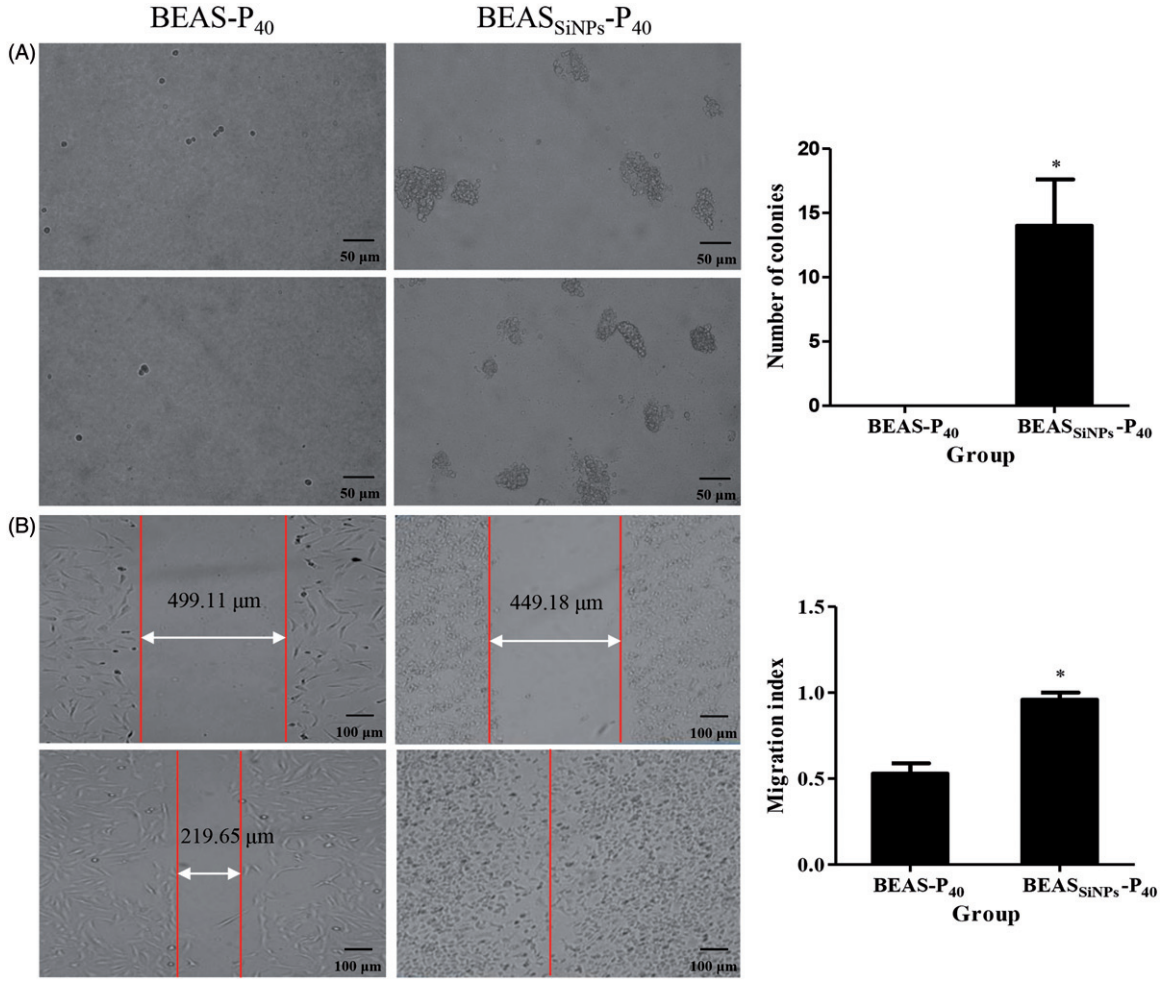

Figure 3. Amorphous SiNPs induce human lung epithelial cell aggressiveness. (A) Anchorage-independent growth on soft agar of $BEAS_{SiNPs}$-P_{40} cells. BEAS-P_{40} and $BEAS_{SiNPs}$-P_{40} cells were seeded on 0.7% agar plates. After four weeks, large colonies (>50 μm in diameter) were formed and clearly observed in $BEAS_{SiNPs}$-P_{40} group, and the number of large colonies was counted under a light microscope. The Scale bar, 50 μm. (B) Representative phase-contrast images (100×) showed an enhanced migration ability of $BEAS_{SiNPs}$-P_{40} cells vs. BEAS-P_{40} acquired from wound healing assay. The Scale bar, 100 μm. Meanwhile, bars represent the migration index of each group, expressed as a value relative to the distance moved by the cell monolayer. Data are means ± SD from three independent experiments. *$p < 0.05$ vs. BEAS-P_{40}.

tumorigenicity of SiNPs-transformed cells, which provided experiment evidence for the carcinogenesis of amorphous SiNPs.

The differentially expressed genes associated with chronic amorphous SiNPs exposure

Hierarchical cluster analysis showed 821 significant differentially expressed genes were triggered by chronic amorphous SiNPs exposure, including 5 up-regulated and 816 down-regulated genes (Figure 5). The differentially expressed genes in amorphous SiNPs-transformed cells are listed in supplementary material Table S4. The data has been deposited in the Gene Expression Omnibus (GEO) repository and are accessible through GEO Series accession number GSE82062.

Functional and pathway analysis of the differentially expressed genes associated with chronic amorphous SiNPs exposure

Go analysis of these differential expression genes identified cell cycle, apoptosis, oxidative stress, cellular division and proliferation, DNA damage, and repair as the prominently perturbed biological functions in response to amorphous SiNPs exposure, which promoted normal cells converted to be malignant (Figure 6(A)). Based on KEGG database, the significant pathway analysis revealed that among 12 down-regulation significant pathways, oxidative phosphorylation, cell cycle, DNA repair including base excision repair, nucleotide excision repair, Mismatch repair, and also p53 and MAPK signaling pathway were directly related to carcinogenesis of amorphous SiNPs (Figure 6(B)).

Signal-net analysis of amorphous SiNPs-transformed human lung epithelial cells

Signal-Net analysis was used to locate core key regulatory genes that had a stronger capacity to modulate adjacent genes. A total of 208 key genes were identified in the transduction network. Genes with higher degrees occupy more important positions within the network. Among them, *TP53* (tumor protein p53) gene was shown to have the highest degrees (Table 2), suggesting *TP53* gene played a

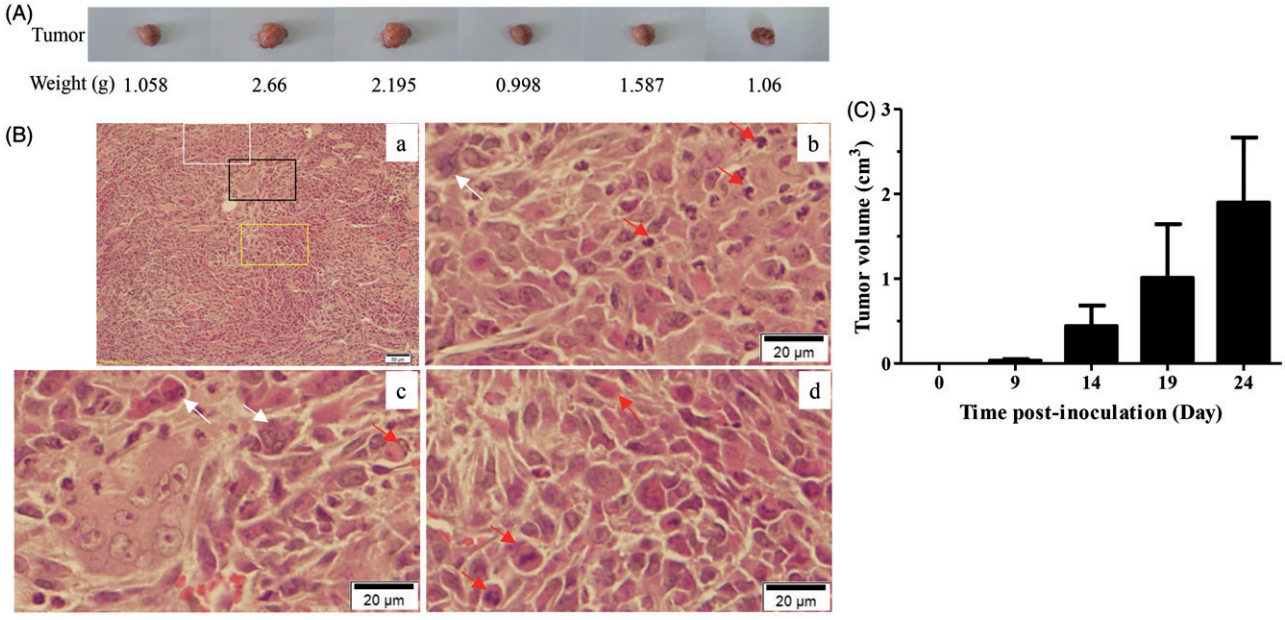

Figure 4. Tumorigenicity of amorphous SiNPs-transformed human lung epithelial cells in nude mice. Nude mice were injected subcutaneously with 1×10^7 $BEAS_{SiNPs}$-P_{40} or BEAS-P_{40} cells. (A) Photographs of tumors formed at the site of injections in mice receiving $BEAS_{SiNPs}$-P_{40} cells at 24 d post-inoculation. However, none of the six mice injected with BEAS-P_{40} cells formed tumor. The weight of tumor tissues was 1.058, 2.66, 2.195, 0.998, 1.587, and 1.06 g, respectively. (B) Tumor tissue samples from $BEAS_{SiNPs}$-P_{40} mice for cell morphology analysis by histological H&E staining with the magnification of 200 × (a). (b–d) represent the amplification of selected area in white, black, and yellow boxes, respectively. The red arrows indicated pathologically abnormal nuclei, and the white arrows showed bi- and multi-nucleated cells, an indicator of mitotic dysfunction. The Scale bar, 50 or 20 μm. (C) Tumor size was quantified at day 9, 14, 19 and 24 after the inoculation of $BEAS_{SiNPs}$-P_{40} cells. Data are means ± SD of triplicate experiments.

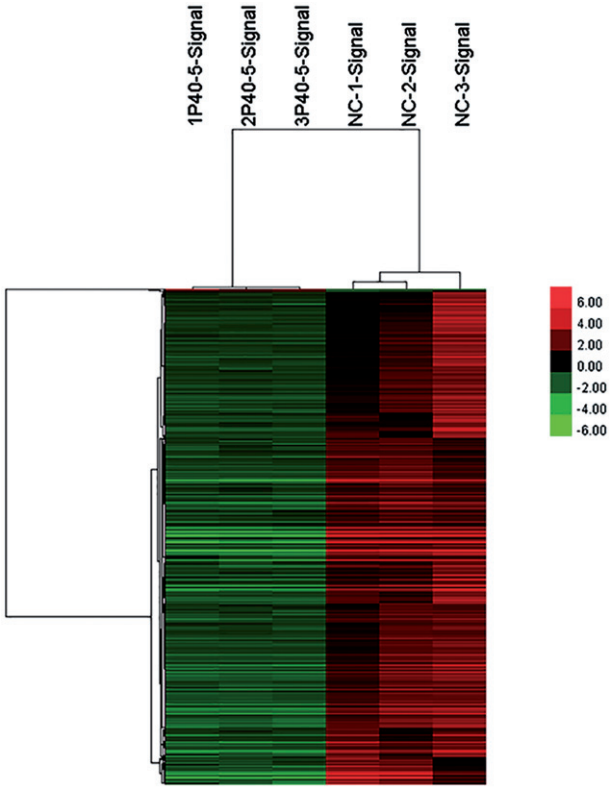

Figure 5. Hierarchical cluster analysis of 821 differential expression genes in human lung epithelial cells chronically exposed to amorphous SiNPs. NC represents for BEAS-P_{40} cells; P40-5 for $BEAS_{SiNPs}$-P_{40} cells. Hierarchical cluster analysis of 821 differential expression genes in human lung epithelial cells chronically exposed to amorphous SiNPs. NC represents for BEAS-P_{40} cells; P40-5 for $BEAS_{SiNPs}$-P_{40} cells. The differentially expressed genes were considered to be up- or down-regulated with 2-fold change and at least $p < 0.05$.

vital role in the transformation process triggered by amorphous SiNPs.

p53 signaling in amorphous SiNPs-transformed human lung epithelial cells

Based on the prediction *via* Signal-Net analysis, the role of tumor suppressor p53 in amorphous SiNPs-transformed cells was determined. The qRT-PCR results revealed that the mRNA expression of p53 was increased firstly, and then marked declined in response to the chronic exposure of amorphous SiNPs (Figure 7(A)). Phosphorylation of p53, an indicator for p53 activation, is regarded as the first crucial step of p53 stabilization (Kruse and Gu 2009). The protein expressions of total p53 and its phosphorylated levels were all down-regulated in $BEAS_{SiNPs}$-P_{40} cells when compared to BEAS-P_{40} (Figure 7(B)). Based on the microarray data, GADD45B, CCNG1, SERPINE1, THBS1, SFN, TP53, CDK4, and CCNB1 were included in p53 signaling pathway (Figure 7(C)). Except for that of CDK4, expressions of all other genes involved in p53 signaling pathway were significantly declined in $BEAS_{SiNPs}$-P_{40} when compared to BEAS-P_{40} cells (Figure 7(D)). All these results confirmed an inactivated p53 signaling pathway in amorphous SiNPs-transformed lung epithelial cells.

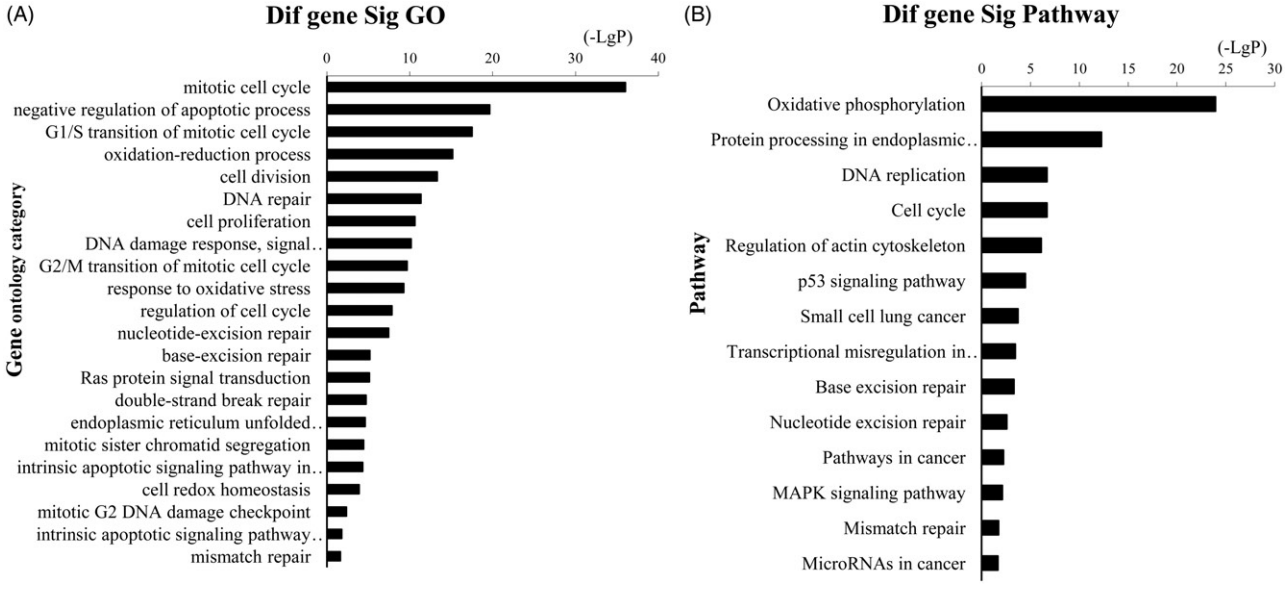

Figure 6. Significantly changed GO and pathways of differentially expressed genes. (A) The downGOs targeted by amorphous SiNPs. (B) Significant pathways of differentially expressed down-regulated genes based on the KEGG database. −LgP, negative logarithm of the *p* value. The larger − LgP indicated a smaller *p* value.

Table 2. The top genes ranked by degree over 5 after signal-net analysis.

Gene symbol	Gene description	Betweenness centrality	Degree	Indegree	Outdegree	*p* Value	Style
TP53	Homo sapiens tumor protein p53 (TP53), transcript variant 1, mRNA.	0.17	32	14	18	1.47×10^{-4}	Down
ACTG1	Homo sapiens actin, gamma 1 (ACTG1), transcript variant 1, mRNA.	7.46×10^{-2}	17	15	9	$<1.00 \times 10^{-7}$	Down
PCNA	Homo sapiens proliferating cell nuclear antigen (PCNA), transcript variant 1, mRNA.	4.12×10^{-2}	17	9	8	2.47×10^{-4}	Down
MEPCE	Homo sapiens methylphosphate capping enzyme (MEPCE), transcript variant 2, mRNA.	5.13×10^{-2}	16	7	9	8.00×10^{-7}	Down
RUVBL2	Homo sapiens RuvB-like 2 (*E. coli*) (RUVBL2), mRNA.	9.50×10^{-2}	10	6	4	4.00×10^{-7}	Down
PLK1	Homo sapiens polo-like kinase 1 (PLK1), mRNA.	3.19×10^{-2}	10	3	7	1.49×10^{-5}	Down
ITGB4	Homo sapiens integrin, beta 4 (ITGB4), transcript variant 1, mRNA.	1.39×10^{-2}	10	9	6	3.08×10^{-5}	Down
ITGB1	Homo sapiens integrin, beta 1 (fibronectin receptor, beta polypeptide, antigen CD29 includes MDF2, MSK12) (ITGB1), transcript variant 1A, mRNA.	9.99×10^{-3}	10	8	7	7.15×10^{-4}	Down
ITGA3	Homo sapiens integrin, alpha 3 (antigen CD49C, alpha 3 subunit of VLA-3 receptor) (ITGA3), transcript variant a, mRNA.	5.53×10^{-3}	10	8	7	1.60×10^{-4}	Down
CCNB1	Homo sapiens cyclin B1 (CCNB1), mRNA.	6.45×10^{-2}	9	5	4	2.26×10^{-3}	Down
ACTN1	Homo sapiens actinin, alpha 1 (ACTN1), transcript variant 2, mRNA.	1.91×10^{-2}	8	7	5	6.56×10^{-3}	Down
GAPDH	Homo sapiens glyceraldehyde-3-phosphate dehydrogenase (GAPDH), transcript variant 1, mRNA.	3.30×10^{-2}	7	3	5	1.00×10^{-7}	Down
XRCC5	Homo sapiens X-ray repair complementing defective repair in Chinese hamster cells 5 (double-strand-break rejoining) (XRCC5), mRNA.	1.57×10^{-2}	7	6	1	2.68×10^{-4}	Down
XRCC6	Homo sapiens X-ray repair complementing defective repair in Chinese hamster cells 6 (XRCC6), mRNA.	6.45×10^{-3}	7	5	2	8.49×10^{-4}	Down
HSPA8	Homo sapiens heat shock 70 kDa protein 8 (HSPA8), transcript variant 1, mRNA.	5.04×10^{-3}	7	3	4	7.44×10^{-4}	Down
TK1	Homo sapiens thymidine kinase 1, soluble (TK1), mRNA.	4.83×10^{-2}	6	4	4	2.00×10^{-7}	Down
THBS1	Homo sapiens thrombospondin 1 (THBS1), mRNA.	2.09×10^{-2}	6	1	5	5.06×10^{-4}	Down
EIF6	Homo sapiens eukaryotic translation initiation factor 6 (EIF6), transcript variant 1, mRNA.	1.33×10^{-2}	6	3	3	$<1.00 \times 10^{-7}$	Down
AURKA	Homo sapiens aurora kinase A (AURKA), transcript variant 1, mRNA.	1.22×10^{-2}	6	3	3	1.41×10^{-3}	Down
RPA1	Homo sapiens replication protein A1, 70 kDa (RPA1), mRNA.	8.94×10^{-3}	6	5	1	1.71×10^{-2}	Down
H2AFX	Homo sapiens H2A histone family, member X (H2AFX), mRNA.	6.76×10^{-3}	6	2	4	1.16×10^{-5}	Down
FLNA	Homo sapiens filamin A, alpha (FLNA), transcript variant 1, mRNA.	1.43×10^{-3}	6	3	6	8.73×10^{-5}	Down
FLNB	Homo sapiens filamin B, beta (FLNB), transcript variant 1, mRNA.	1.43×10^{-3}	6	4	5	2.36×10^{-3}	Down
BABAM1	Homo sapiens BRISC and BRCA1 A complex member 1 (BABAM1), transcript variant 1, mRNA.	0	6	0	6	2.00×10^{-6}	Down
POLR2E	Homo sapiens polymerase (RNA) II (DNA directed) polypeptide E, 25 kDa (POLR2E), mRNA.	8.20×10^{-2}	5	3	2	2.83×10^{-4}	Down
DCTPP1	Homo sapiens dCTP pyrophosphatase 1 (DCTPP1), mRNA.	2.62×10^{-2}	5	5	4	$<1.00 \times 10^{-7}$	Down
TRIM28	Homo sapiens tripartite motif containing 28 (TRIM28), mRNA.	2.15×10^{-2}	5	3	2	3.10×10^{-6}	Down
APEX1	Homo sapiens APEX nuclease (multifunctional DNA repair enzyme) 1 (APEX1), transcript variant 4, mRNA.	9.12×10^{-3}	5	2	3	2.40×10^{-3}	Down
HLA-B	Homo sapiens major histocompatibility complex, class I, B (HLA-B), mRNA.	7.53×10^{-3}	5	4	4	7.00×10^{-7}	Down
CCNA2	Homo sapiens cyclin A2 (CCNA2), mRNA.	6.02×10^{-3}	5	2	3	5.29×10^{-3}	Down
MED31	Homo sapiens mediator complex subunit 31 (MED31), mRNA.	5.64×10^{-3}	5	3	2	1.78×10^{-5}	Down
PTTG1	Homo sapiens pituitary tumor-transforming 1 (PTTG1), mRNA.	5.44×10^{-3}	5	2	3	2.69×10^{-3}	Down
E2F1	Homo sapiens E2F transcription factor 1 (E2F1), mRNA.	4.12×10^{-3}	5	3	2	1.10×10^{-6}	Down
FN1	Homo sapiens fibronectin 1 (FN1), transcript variant 3, mRNA.	2.26×10^{-3}	5	1	4	2.17×10^{-3}	Down
ACTN4	Homo sapiens actinin, alpha 4 (ACTN4), mRNA.	1.00×10^{-3}	5	5	4	2.26×10^{-3}	Down
EIF3F	Homo sapiens eukaryotic translation initiation factor 3, subunit F (EIF3F), mRNA.	8.30×10^{-5}	5	2	3	2.11×10^{-4}	Down
RHOA	Homo sapiens Ras homolog family member A (RHOA), mRNA.	0	5	0	5	3.16×10^{-5}	Down

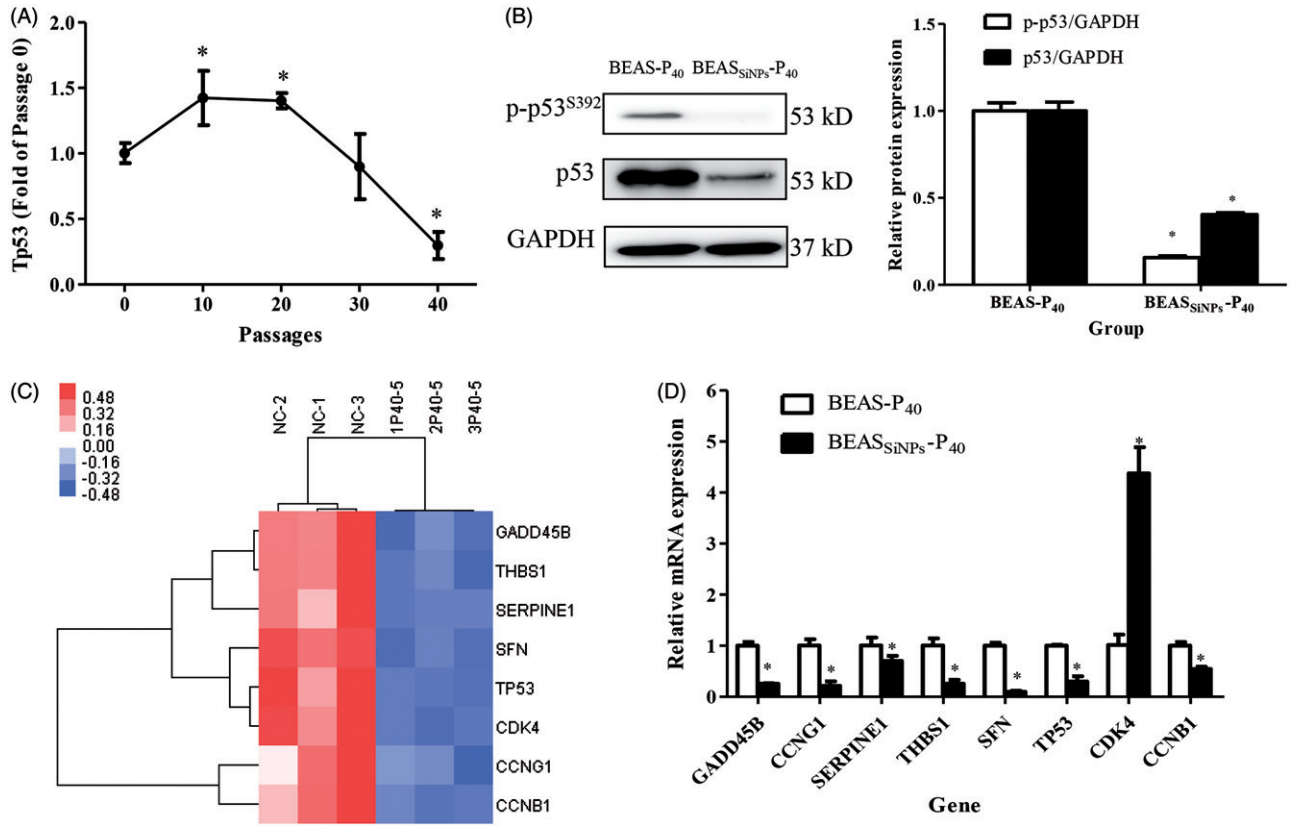

Figure 7. Amorphous SiNPs induce inactivation of p53 and its signaling pathway in human lung epithelial cells. (A) Expression of p53 mRNA level, which increased on the 10th and 20th passage, and marked declined on the 40th passage when compared to the passage 0 ($^*p < 0.05$). (B) Western blot assay showed a significant decline of the total- and phosphor-p53 after chronic exposure to amorphous SiNPs. All blots shown are representative of three independent experiments. Relative densitometric analysis of the protein bands was also performed and presented. (C) Hierarchical cluster analysis of differently expressed genes belonging to p53 signaling pathway in $BEAS_{SiNPs}$-P_{40} cells. (D) qRT-PCR analysis showed the gene expressions of GADD45B, CCNG1, SERPINE1, THBS1, SFN, TP53, and CCNB1 were significantly decreased except for that of CDK4. Data are expressed as means ± SD from three independent experiments. $^*p < 0.05$ vs. BEAS-P_{40}.

Discussion

The *in vitro* cell transformation assay has been regarded as a appropriate approach with established relevance, reliability and reproducibility for the evaluation of potential carcinogens (Lilienblum et al. 2008). For the evaluation of the potential carcinogenicity of amorphous SiNPs on lung tissue, ideally, primary lung cells should be used. However, the short lifespan of these primary cultures is not compatible with prolonged exposures to low amorphous SiNPs-doses. For this reason, the immortalized human lung epithelial cell line, BEAS-2B (SV40 immortalized) was the option. Some findings suggested that the immortalization by SV40, which leads to the sequestration of p53 (Lehman et al. 1993), may induce malignant transformation. Nevertheless, the contrast confirmed that immortalization by SV40 was not sufficient for the malignant transformation of Beas-2B cells (Rodrigues et al. 2009), since non-treated Beas-2B cells are nonmalignant as evidences by *in vitro* cell transformation assay and *in vivo* xenograft tumor model (Ramirez et al. 2004). To date, accumulating reports investigate the carcinogenesis of chemicals and related mechanisms by using malignant transformation assay in Beas-2B cells (Yao et al. 2015; Wang et al. 2016). Rodrigues et al. had ever suggested that the Cr(VI)-induced *in vitro* malignant transformation of Beas-2B cells was similar to their *in vivo* human bronchial pre-neoplastic and malignant lesions (Rodrigues et al. 2009). Beas-2B cells have been widely applied for the *in vitro* carcinogenicity evaluation of other nanomaterials (Wang et al. 2011; Luanpitpong et al. 2014; Vales, Rubio, and Marcos 2015; Choo et al. 2016) and also for that of crystalline silica (Antognelli et al. 2016). Thereby, the *in vitro* transformation model of BEAS-2B has been

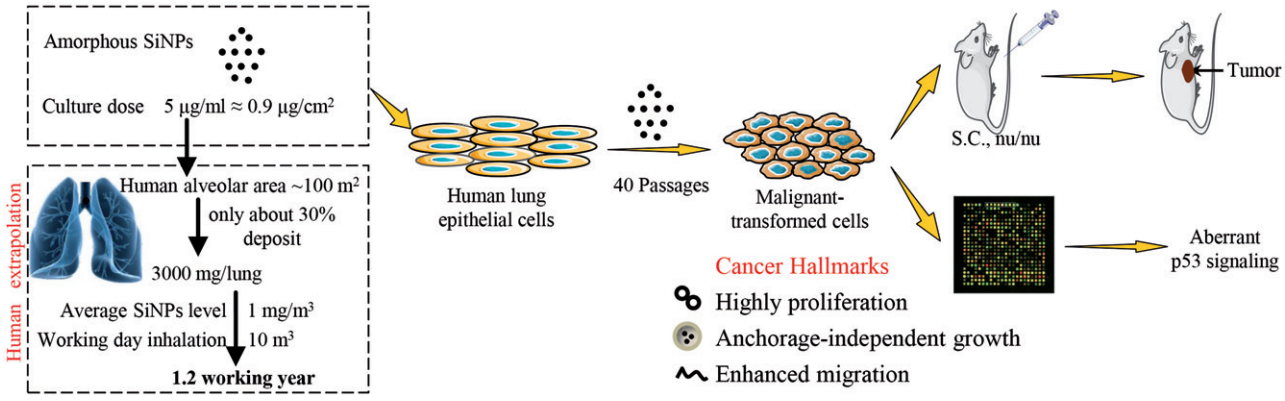

Figure 8. Schematic model of amorphous SiNPs-induced malignant transformation and tumorigenesis of human lung epithelial cells via p53 signaling. Additionally, the extrapolation of amorphous SiNPs dose in cell culture model to human exposure scenarios in the workplace was shown in left part. Consequently, the chronic interaction between the depository amorphous SiNPs and lung epithelial cells induced cellular malignant transformation, which was probably mediated by the aberrant p53 signaling.

suggested as a screening assay for the carcinogenic potential of engineered NPs. Still, it remains to carry out several improvements to enhance the specificity and sensitivity of the test.

Up to now, quite a large quantity of researches reported the cyto- and geno-toxicity of amorphous SiNPs, but there is still no conclusive information on its carcinogenic potential. So far, there are no epidemiological studies looking specifically for amorphous SiNPs carcinogenicity on humans, and no adequate animal data to clarify the possible mechanisms of action. For this reason, the Beas-2B cells were chronically exposed to low- and non-cytotoxic dose (5 μg/mL) of amorphous SiNPs for 40 passages, and their malignant transformation was assessed. A short-term amorphous SiNPs exposure (100 μg/mL, 72 h) did not induce morphological transformation of Balb/3T3 mouse fibroblasts. On the contrary, our amorphous SiNPs-treated cells manifested remarkable alterations in cellular morphology, proliferation, cell cycle, migration and invasion, commonly associated with malignant transformation. Moreover, when the obtained cells were injected into nude mice, it induced tumors. By the way, we did cell line authentication test for $BEAS_{SiNPs}$-P_{40} and BEAS-P_{40} cells (Supplemental file). Particle loading into the lungs is essential to the NPs' pulmonary toxicological study. For the carcinogenic evaluation, chronic exposure and environmentally or occupationally relevant doses should be taken into consideration. To date, the occupation exposure limits (OELs) of SiNPs has not been established by the National Institute for Occupational Safety and Health (NIOSH) and the data available on its occupational exposure is also insufficient. It has been reported that the occupational exposure level of silica nanoparticles ranged from 1.0 to 27.6 mg/m^3 (Kim, Kim, and Yu 2014; Oh, Kim, and Kim 2014; Debia et al. 2016). Based on a previous report (Luanpitpong et al. 2014), the amorphous SiNPs doses used in the *in vitro* exposure is equivalent to a human lung burden for 8 h/d about two weeks at 27.6 mg/m^3 (high level) or about 1.2 years at 1.0 mg/m^3 (average level). The extrapolation of amorphous SiNPs dose in cell culture model to human exposure scenarios in the workplace was depicted in Figure 8. Consistent with our notion, an *in vivo* long-term toxicology study of SiNPs at realistic exposure level was conducted, in which the dosage is set up as 2.6 ± 0.6 and 10.6 ± 2.1 mg/m^3 (Sutunkova et al. 2017). Interestingly, they observed a low systemic toxicity and negligible pulmonary fibrogenicity, which may be attributed to low particle retention in lungs due to the relatively high solubility of these particles. However, these particles manifested systemic genotoxic action in the rat organism. Additionally, a recent study observed that at normal atmospheric condition, SiNPs existed not with the expected classical composition SiO_2 postulated by classical chemistry, but in an oxygen-enriched form (Lepeshkin et al. 2016), which may contributed to the known high carcinogenicity of silica dust. All in all, exposure scenario, model, dose, physiochemical properties of particles, etc., should be considered for an

overall, rational evaluation of the NPs' carcinogenic potential, which could well-explain the obtained controversial results by different investigators.

Carcinogenesis is a multistep process involving mutation and the subsequent selective clonal expansion of the mutated cell. Oxidative stress induced by SiNPs has long been recognized as major contributor to oxidative injury and DNA damage (Gong et al. 2012; Tarantini et al. 2015), thus accelerating the rate of cancer-causing mutations. That would agree with our data demonstrating amorphous SiNPs-induced malignant transformation in BEAS-2B cells mainly associated with oxidative stress and genotoxicity, eventually contributing to carcinogenesis (Figure 6). Several studies revealed the critical role of oxidative stress in amorphous SiNPs induced cytotoxicity to human lung epithelial cells (Eom and Choi 2009, 2011; Lin et al. 2016). Definitely, chronic oxidative stress caused malignant transformation of mammary epithelial cells along with stimulating multiple signaling pathways (Mori, Shibanuma, and Nose 2004). Constitutive activation of Nrf2 (NF-E2-related factor 2), a critical cellular defense mechanism against oxidative stress, contributed to malignant transformation in human lung epithelial cells (Yang et al. 2015), and is closely associated with cancer development, progression, and chemotherapy resistance (Pi et al. 2008). The dynamic changes of Nrf2 and its target antioxidant genes were observed in our test (supplementary Figure S3). Classically, the development of cancer is largely associated with inherited or acquired mutations of specific genes that regulate cell cycle, proliferation, and apoptosis (Stratton, Campbell, and Futreal 2009; Vogelstein et al. 2013). Excess ROS can direct attack to DNA, resulting in a variety of DNA lesions, oncogenic mutations, and ultimately leading to genomic instability (Trachootham, Alexandre, and Huang 2009). Our previous studies revealed oxidative DNA damage by amorphous SiNPs exposure (Li et al. 2011; Yu et al. 2015b). Down-regulation of base excision repair, nucleotide excision repair, and mismatch repair by amorphous SiNPs contributes to oxidative DNA damage and subsequent genomic instability (Kovvuru et al. 2015), which may explain the maintenance of mutant cells to survive and proliferation, eventually leading to tumor. p53 is involved in the maintenance of genome stability, whereas p53 inactivation is a common characteristic of tumors (Aylon and Oren 2007; Kastan 2007). Previous studies have demonstrated a critical role of p53 in NPs-induced carcinogenesis (Takagi et al. 2008; Wang et al. 2011). BEAS-2B cells possess wtp53 and also a mutated $p53^{Ser47}$ gene (Gerwin et al. 1992). As predicted by signal-net analysis, p53 was the most important regulator in amorphous SiNPs-induced malignant transformation of BEAS-2B cells (Table 2). It has been well-documented that activation of p53 regulates SiNPs-induced short-term toxicity (Liu and Sun 2010; Ahmad et al. 2012). That may well explain the initially activation of p53 was coincident with the observation upon short-term SiNPs exposure. Nevertheless, the later p53 signaling inactivation may lead to the loss of its corrective power, but also promoting conversion of normal cells into malignant, and ultimately cancer (Park et al. 2015). Similarly, chronic exposure to silver NPs (0.13 or 1.33 μg/mL, 40 passages) also manifested an inhibition on p53 mRNA level and p-p53 expression (Choo et al. 2016). Vormer et al. reported that the partial ablation of p53 pathway strongly stimulated anchorage-independent growth of mouse embryonic fibroblasts (Vormer et al. 2008). All these results confirmed an inactivated p53 and its signaling pathway in amorphous SiNPs-transformed lung epithelial cells, which probably contributed to tumor initiation and progression through a combination of increased genetic instability, loss of growth-arresting signals, and inappropriate cell survival (Park et al. 2015). In addition, epigenetic alterations also involved in chronically low-dose amorphous SiNPs-exposed BEAS-2B cells (Zou et al. 2016). There is growing evidence that the p53 protein enforces fidelity of the epigenetic program, and the inactivation or loss of *p53* gene functions increase the probability to alter the epigenetic landscape of the genome in cancerous cells (Levine et al. 2016). Therefore, genetic and also epigenetic mechanisms existing in the malignant cell transformation process induced by amorphous SiNPs need to be further investigated.

Conclusions

In summary, our study firstly demonstrated that the chronic exposure to low-dose amorphous SiNPs can cause malignant transformation of human lung epithelial cells as demonstrated by the enhanced

cellular proliferation, colony formation, and increased cell migration, as well as the induction of tumorigenesis in nude mice. These results indicated the *in vitro* carcinogenic potential of chronic amorphous SiNPs exposure, which has not been well addressed and is of great concern. Our data also provided a comprehensive understanding of genome-wide transcriptional analysis of amorphous SiNPs-induced malignant transformation, and indicated loss of p53 function, including aberrant p53 signaling and inactivated p53, as a potential mechanism for amorphous SiNPs-induced malignant transformation, consistent with the previous observations that most human cancers have p53 tumor suppressor gene inactivation. A schematic model of the amorphous SiNPs-induced malignant transformation and tumorigenesis of human lung epithelial cells *via* p53 signaling was presented in Figure 8. Further study is required to verify the underlying mechanisms involved in this transformation process induced by amorphous SiNPs.

Acknowledgments

The authors thank Prof. Wensheng Yang from Jilin University for the preparation of the SiNPs, and Weiping Tang of Cnkingbio biotechnology Co. Ltd for bioinformatics assistance.

Disclosure statement

The authors declare they have no conflict of interest.

Funding

This work was supported by National Natural Science Foundation of China (No. 81202242, No. 81573176), General Program of Beijing Natural Science Foundation (7162021, 7162022); Science and Technology Development Program of the Beijing Municipal Commission of Education (KM201510025005).

References

Ahamed, M. 2013. "Silica Nanoparticles-Induced Cytotoxicity, Oxidative Stress and Apoptosis in Cultured A431 and A549 Cells." *Human & Experimental Toxicology* 32: 186–195. doi: 10.1177/0960327112459206.

Ahmad, J., M. Ahamed, M. J. Akhtar, S. A. Alrokayan, M. A. Siddiqui, J. Musarrat, and A. A. Al-Khedhairy. 2012. "Apoptosis Induction by Silica Nanoparticles Mediated Through Reactive Oxygen Species in Human Liver Cell Line HepG2." *Toxicology and Applied Pharmacology* 259: 160–168. doi:10.1016/j.taap.2011.12.020.

Akhtar, J., Z. Wang, C. Yu, and Z. P. Zhang. 2014. "Effectiveness of Local injection of Lentivirus-Delivered Stathmin1 and Stathmin1 shRNA in Human Gastric Cancer Xenograft Mouse." *Journal of Gastroenterology and Hepatology* 29: 1685–1691. doi: 10.1111/jgh.12594.

Anon. 1997. "IARC Working Group on the Evaluation of Carcinogenic Risks to Humans: Silica, Some Silicates, Coal Dust and Para-Aramid Fibrils. Lyon, 15–22 October 1996." *IARC Monographs on the Evaluation of Carcinogenic Risks to Humans* 68: 1–475. https://www.ncbi.nlm.nih.gov/books/NBK410047/.

Antognelli, C., A. Gambelunghe, G. Muzi, and V. N. Talesa. 2016. "Glyoxalase I Drives Epithelial-to-Mesenchymal Transition via Argpyrimidine-Modified Hsp70, Mir-21 And SMAD Signalling in Human Bronchial Cells BEAS-2B Chronically Exposed to Crystalline Silica Min-U-Sil 5: Transformation into a Neoplastic-Like Phenotype." *Free Radical Biology & Medicine* 92: 110–125. doi: 10.1016/j.freeradbiomed.2016.01.009.

Aylon, Y., and M. Oren. 2007. "Living with p53, Dying of p53." *Cell* 130: 597–600. doi: 10.1016/j.cell.2007.08.005.

Bakand, S., A. Hayes, and F. Dechsakulthorn. 2012. "Nanoparticles: A Review of Particle Toxicology Following Inhalation Exposure." *Inhalation Toxicology* 24: 125–135. doi:10.3109/08958378.2010.642021.

Benigni, R., C. Bossa, and O. Tcheremenskaia. 2013. "In Vitro Cell Transformation Assays for an Integrated, Alternative Assessment of Carcinogenicity: A Data-Based Analysis." *Mutagenesis* 28: 107–116. doi: 10.1093/mutage/ges059.

Borak, B., P. Biernat, A. Prescha, A. Baszczuk, and J. Pluta. 2012. "In Vivo Study on the Biodistribution of Silica Particles in the Bodies of Rats." *Advances in Clinical and Experimental Medicine: Official Organ Wroclaw Medical University* 21: 13–18. http://www.advances.umed.wroc.pl/en/article/2012/21/1/13/.

Cho, S. Y., and R. L. Klemke. 2000. "Extracellular-Regulated Kinase Activation and CAS/Crk Coupling Regulate Cell Migration and Suppress Apoptosis During Invasion of the Extracellular Matrix." *The Journal of Cell Biology* 149: 223–236. doi:10.1083/jcb.149.1.223.

Cho, W.-S., M. Choi, B. S. Han, M. Cho, J. Oh, K. Park, S. J. Kim, et al. 2007. "Inflammatory Mediators Induced by Intratracheal Instillation of Ultrafine Amorphous Silica Particles." *Toxicology Letters* 175: 24–33. doi:10.1016/j.toxlet.2007.09.008.

Choi, M., W. Cho, B. Han, M. Cho, S. Kim, J. Yi, B. Ahn, et al. 2008. "Transient Pulmonary Fibrogenic Effect Induced by Intratracheal Instillation of Ultrafine Amorphous Silica in A/J Mice." *Toxicology Letters* 182: 97–101. doi:10.1016/j.toxlet.2008.08.019.

Choo, W. H., C. H. Park, S. E. Jung, B. Moon, H. Ahn, J. S. Ryu, K.-S. Kim, et al. 2016. "Long-Term Exposures to Low Doses of Silver Nanoparticles Enhanced *in vitro* Malignant Cell Transformation in Non-tumorigenic BEAS-2B Cells." *Toxicology In Vitro: An International Journal Published*

in Association with Bibra 37: 41–49. doi:10.1016/j.tiv.2016.09.003.

Couto, S. S., S. M. Griffey, P. C. Duarte, and B. R. Madewell. 2002. "Feline Vaccine-Associated Fibrosarcoma: Morphologic Distinctions." *Veterinary Pathology* 39: 33–41. doi:10.1354/vp.39-1-33.

Cox, A. D., and C. J. Der. 1994. "Biological assays for cellular transformation." *Methods in Enzymology* 238: 277–294. doi:10.1016/0076-6879(94)38026-0.

Darne, C., C. Coulais, F. Terzetti, C. Fontana, S. Binet, L. Gaté, Y. Guichard, et al. 2016. "*In Vitro* Comet and Micronucleus Assays Do Not Predict Morphological Transforming Effects of Silica Particles in Syrian Hamster Embryo Cells." *Mutation Research/Genetic Toxicology and Environmental Mutagenesis* 796: 23–33. doi:10.1016/j.mrgentox.2015.11.012.

Debia, M., B. Bakhiyi, C. Ostiguy, J. H. Verbeek, D. H. Brouwer, and V. Murashov. 2016. "A Systematic Review of Reported Exposure to Engineered Nanomaterials." *The Annals of Occupational Hygiene* 60: 916–935. doi:10.1093/annhyg/mew041.

Deeble, P. D., M. E. Cox, H. F. Frierson, R. A. Sikes, J. B. Palmer, R. J. Davidson, E. V. Casarez, et al. 2007. "Androgen-Independent Growth and Tumorigenesis of Prostate Cancer Cells are Enhanced by the Presence of PKA-Differentiated Neuroendocrine Cells." *Cancer Res* 67: 3663–3672. doi:10.1158/0008-5472.CAN-06-2616.

Du, Z., D. Zhao, L. Jing, G. Cui, M. Jin, Y. Li, X. Liu, et al. 2013. "Cardiovascular Toxicity of Different Sizes Amorphous Silica Nanoparticles in Rats After Intratracheal Instillation." *Cardiovascular Toxicology* 13: 194–207. doi:10.1007/s12012-013-9198-y.

Elias, Z., O. Poirot, M. C. Danière, F. Terzetti, A. M. Marande, S. Dzwigaj, H. Pezerat, et al. 2000. "Cytotoxic and Transforming Effects of Silica Particles with Different Surface Properties in Syrian Hamster Embryo (SHE) Cells." *Toxicology in Vitro: An International Journal Published in Association with Bibra* 14: 409–422. doi:10.1016/S0887-2333(00)00039-4.

Elias, Z., O. Poirot, I. Fenoglio, M. Ghiazza, M.-C. Danière, F. Terzetti, C. Darne, et al. 2006. "Surface Reactivity, Cytotoxic, and Morphological Transforming Effects of Diatomaceous Earth Products in Syrian Hamster Embryo Cells." *Toxicological Sciences: An Official Journal of the Society of Toxicology* 91: 510–520. doi:10.1093/toxsci/kfj177.

Eom, H. J., and J. Choi. 2009. "Oxidative Stress of Silica Nanoparticles in Human Bronchial Epithelial Cell, Beas-2B." *Toxicology In Vitro: An International Journal Published in Association with Bibra* 23: 1326–1332. doi:10.1016/j.tiv.2009.07.010.

Eom, H. J., and J. Choi. 2011. "SiO(2) Nanoparticles Induced Cytotoxicity by Oxidative Stress in Human Bronchial Epithelial Cell, Beas-2B." *Environmental Health and Toxicology* 26: e2011013. doi: 10.5620/eht.2011.26.e2011013.

Fubini, B., I. Fenoglio, Z. Elias, and O. Poirot. 2001. "Variability of Biological Responses to Silicas: Effect of Origin, Crystallinity, and State of Surface on Generation of Reactive Oxygen Species and Morphological Transformation of Mammalian Cells." *Journal of Environmental Pathology, Toxicology and Oncology* 20: 95–108. doi:10.1615/JEnvironPatholToxicolOncol.v20.iSuppl.1.90.

Gao, A., S. Song, X. Zuo, W. Guo, P. Niu, and L. Tian. 2010. "Epigenetic Mediated Transcriptional Activation of PARP-1 Participates in Silica-Associated Malignant Transformation of Human Bronchial Epithelial Cells." *Toxicology Letters* 193: 236–241. doi:10.1016/j.toxlet.2010.01.017.

Gatoo, M. A., S. Naseem, M. Y. Arfat, A. M. Dar, K. Qasim, and S. Zubair. 2014. "Physicochemical Properties of Nanomaterials: Implication in Associated Toxic Manifestations." *Biomed Research International* 2014: 498420. doi:10.1155/2014/498420.

Gehrke, H., A. Frühmesser, J. Pelka, M. Esselen, L. L. Hecht, H. Blank, H. P. Schuchmann, et al. 2013. "*In Vitro* Toxicity of Amorphous Silica Nanoparticles in Human Colon Carcinoma Cells." *Nanotoxicology* 7: 274–293. doi:10.3109/17435390.2011.652207.

Gerwin, B. I., E. Spillare, K. Forrester, T. A. Lehman, J. Kispert, J. A. Welsh, A. M. Pfeifer, et al. 1992. "Mutant p53 can Induce Tumorigenic Conversion of Human Bronchial Epithelial Cells and Reduce Their Responsiveness to a Negative Growth Factor, Transforming Growth Factor Beta 1." *Proceedings of the National Academy of Sciences of the United States of America* 89: 2759–2763. doi:10.1073/pnas.89.7.2759.

Gilardino, A., F. Catalano, F. A. Ruffinatti, G. Alberto, B. Nilius, S. Antoniotti, G. Martra, et al. 2015. "Interaction of SiO2 Nanoparticles with Neuronal Cells: Ionic Mechanisms Involved in the Perturbation of Calcium Homeostasis." *The International Journal of Biochemistry & Cell Biology* 66: 101–111. doi:10.1016/j.biocel.2015.07.012.

Gong, C., G. Tao, L. Yang, J. Liu, H. He, and Z. Zhuang. 2012. "The Role of Reactive Oxygen Species in Silicon Dioxide Nanoparticle-Induced Cytotoxicity and DNA Damage in HaCaT Cells." *Molecular Biology Reports* 39: 4915–4925. doi:10.1007/s11033-011-1287-z.

Guha, N., K. Straif, and L. Benbrahim-Tallaa. 2011. "The IARC Monographs on the Carcinogenicity of Crystalline Silica." *La Medicina Del Lavoro* 102: 310–320.

Guo, C., Y. Xia, P. Niu, L. Jiang, J. Duan, Y. Yu, X. Zhou, et al. 2015. "Silica Nanoparticles Induce Oxidative stress, Inflammation, and Endothelial Dysfunction *in vitro* via Activation of the MAPK/Nrf2 Pathway and Nuclear Factor-κB Signaling." *International Journal of Nanomedicine* 10: 1463–1477. doi:10.2147/IJN.S76114.

Guo, C., M. Yang, L. Jing, J. Wang, Y. Yu, Y. Li, J. Duan, et al. 2016. "Amorphous Silica Nanoparticles Trigger Vascular Endothelial Cell Injury through Apoptosis and Autophagy via Reactive Oxygen Species-Mediated MAPK/Bcl-2 and PI3K/Akt/mTOR Signaling." *International Journal of Nanomedicine* 11: 5257–5276. doi:10.2147/IJN.S112030.

Hou, S., S. Zhou, Z. Qin, L. Yang, X. Han, S. Yao, and H. Ji. 2017. "Evidence, Mechanism, and Clinical Relevance of the Transdifferentiation from Lung Adenocarcinoma to Squamous Cell Carcinoma." *American Journal of Pathology* 187: 954–962. doi:10.1016/j.ajpath.2017.01.009.

Hu, H.,. Q. Li, L. Jiang, Y. Zou, J. Duan, and Z. Sun. 2016. "Genome-Wide Transcriptional Analysis of Silica Nanoparticle-Induced Toxicity in Zebrafish Embryos." *Toxicol Res* 5: 609–620. doi:10.1039/C5TX00383K.

Hristozov, D. R., S. Gottardo, A. Critto, and A. Marcomini. 2012. "Risk Assessment of Engineered Nanomaterials: A Review of Available Data and Approaches from a Regulatory Perspective." *Nanotoxicology* 6: 880–898. doi:10.3109/17435390.2011.626534.

Huang, S., P. J. Chueh, Y. W. Lin, T. S. Shih, and S. M. Chuang. 2009. "Disturbed Mitotic Progression and Genome Segregation are Involved in Cell Transformation Mediated by Nano-TiO2 Long-Term Exposure." *Toxicology and Applied Pharmacology* 241: 182–194. doi:10.1016/j.taap.2009.08.013.

Kastan, M. B. 2007. "Wild-type p53: Tumors can't Stand It." *Cell* 128: 837–840. doi:10.1016/j.cell.2007.02.022.

Kim, B., H. Kim, and I. J. Yu. 2014. "Assessment of Nanoparticle Exposure in Nanosilica Handling Process: Including Characteristics of Nanoparticles Leaking from a Vacuum Cleaner." *Industrial Health* 52: 152–162. doi:10.2486/indhealth.2013-0087.

Kolling, A., H. Ernst, S. Rittinghausen, and U. Heinrich. 2011. "Relationship of Pulmonary Toxicity and Carcinogenicity of Fine and Ultrafine Granular Dusts in a Rat Bioassay." *Inhalation Toxicology* 23: 544–554. doi:10.3109/08958378.2011.594458.

Kovvuru, P., P. E. Mancilla, A. B. Shirode, T. M. Murray, T. J. Begley, and R. Reliene.2015. "Oral Ingestion of Silver Nanoparticles Induces Genomic Instability and DNA Damage in Multiple Tissues." *Nanotoxicology* 9: 162–171. doi:10.3109/17435390.2014.902520.

Kruse, J. P., and W. Gu. 2009. "Modes of p53 Regulation." *Cell* 137: 609–622. doi:10.1016/j.cell.2009.04.050.

Lehman, T. A., R. Modali, P. Boukamp, J. Stanek, W. P. Bennett, J. A. Welsh, R. A. Metcalf, et al. 1993. "p53 Mutations in Human Immortalized Epithelial Cell Lines." *Carcinogenesis* 14: 833–839. doi:10.1093/carcin/14.5.833.

Lepeshkin, S., V. Baturin, E. Tikhonov, N. Matsko, Y. Uspenskii, A. Naumova, O. Feya, et al. 2016. "Super-Oxidation of Silicon Nanoclusters: Magnetism and Reactive Oxygen Species at the Surface." *Nanoscale* 8: 18616–18620. doi:10.1039/c6nr07504e.

Levine, A. J., A. M. Puzio-Kuter, C. S. Chan, and P. Hainaut. 2016. "The Role of the p53 Protein in Stem-Cell Biology and Epigenetic Regulation." *Cold Spring Harbor Perspectives in Medicine* 6: a026153. doi:10.1101/cshperspect.a026153.

Li, Y., L. Sun, M. Jin, Z. Du, X. Liu, C. Guo, Y. Li, et al. 2011. "Size-Dependent Cytotoxicity of Amorphous Silica Nanoparticles in Human Hepatoma HepG2 Cells." *Toxicology in Vitro: An International Journal Published in Association with Bibra* 25: 1343–1352. doi:10.1016/j.tiv.2011.05.003.

Lilienblum, W., W. Dekant, H. Foth, T. Gebel, J. G. Hengstler, R. Kahl, P.-J. Kramer, et al. 2008. "Alternative Methods to Safety Studies in Experimental Animals: Role in the Risk Assessment of Chemicals under the New European Chemicals Legislation (REACH)." *Archives of Toxicology* 82: 211–236. doi:10.1007/s00204-008-0279-9.

Lin, C., X. Zhao, D. Sun, L. Zhang, W. Fang, T. Zhu, Q. Wang, et al. 2016. "Transcriptional Activation of Follistatin by Nrf2 Protects Pulmonary Epithelial Cells Against Silica Nanoparticle-Induced Oxidative Stress." *Scientific Reports* 6: 21133. doi:10.1038/srep21133.

Liu, X., and J. A. Sun. 2010. "Endothelial Cells Dysfunction Induced by Silica Nanoparticles Through Oxidative Stress via JNK/P53 and NF-kappa B Pathways." *Biomaterials* 31: 8198–8209. doi:10.1016/j.biomaterials.2010.07.069.

Luanpitpong, S., L. Wang, V. Castranova, and Y. Rojanasakul. 2014. "Induction of Stem-Like Cells with Malignant Properties by Chronic Exposure of Human Lung Epithelial Cells to Single-Walled Carbon Nanotubes." *Particle and Fibre Toxicology* 11: 22. doi:10.1186/1743-8977-11-22.

Mori, K., M. Shibanuma, and K. Nose. 2004. "Invasive Potential Induced under Long-Term Oxidative Stress in Mammary Epithelial Cells." *Cancer Research* 64: 7464–7472. doi:10.1158/0008-5472.CAN-04-1725.

Mu, Q., N. S. Hondow, L. Krzemiński, A. P. Brown, L. J. C. Jeuken, and M. N. Routledge. 2012. "Mechanism of Cellular Uptake of Genotoxic Silica Nanoparticles." *Particle and Fibre Toxicology* 9: 29. doi:10.1186/1743-8977-9-29.

Napierska, D., L. C. J. Thomassen, D. Lison, J. A. Martens, and P. H. Hoet. 2010. "The Nanosilica Hazard: Another Variable Entity." *Particle and Fibre Toxicology* 7: 39. doi:10.1186/1743-8977-7-39.

Oh, S., B. Kim, and H. Kim. 2014. "Comparison of Nanoparticle Exposures Between Fumed and Sol-gel Nano-silica Manufacturing Facilities." *Industrial Health* 52: 190–198.

Park, M. V. D. Z., H. W. Verharen, E. Zwart, L. G. Hernandez, J. van Benthem, A. Elsaesser, C. Barnes, et al. 2011. "Genotoxicity Evaluation of Amorphous Silica Nanoparticles of Different Sizes Using the Micronucleus and the Plasmid lacZ Gene Mutation Assay." *Nanotoxicology* 5: 168–181. doi:10.3109/17435390.2010.506016.

Park, Y. H., D. Kim, J. Dai, and Z. Zhang. 2015. "Human Bronchial Epithelial BEAS-2B Cells, an Appropriate *in Vitro* Model to Study Heavy Metals Induced Carcinogenesis." *Toxicology and Applied Pharmacology* 287: 240–245. doi:10.1016/j.taap.2015.06.008.

Pi, J., B. A. Diwan, Y. Sun, J. Liu, W. Qu, Y. He, M. Styblo, et al. 2008. "Arsenic-Induced Malignant Transformation of Human Keratinocytes: Involvement of Nrf2." *Free Radical Biology & Medicine* 45: 651–658. doi:10.1016/j.freeradbiomed.2008.05.020.

Ramirez, R. D., S. Sheridan, L. Girard, M. Sato, Y. Kim, J. Pollack, M. Peyton, et al. 2004. "Immortalization of Human

Bronchial Epithelial Cells in the Absence of Viral Oncoproteins." *Cancer Research* 64: 9027–9034. doi:10.1158/0008-5472.CAN-04-3703.

Rodrigues, C. F. D., A. M. Urbano, E. Matoso, I. Carreira, A. Almeida, P. Santos, F. Botelho, et al. 2009. "Human Bronchial Epithelial Cells Malignantly Transformed by Hexavalent Chromium Exhibit an Aneuploid Phenotype but No Microsatellite Instability." *Mutation Research* 670: 42–52. doi:10.1016/j.mrfmmm.2009.07.004.

Sergent, J. A., V. Paget, and S. Chevillard. 2012. "Toxicity and Genotoxicity of Nano-SiO2 on Human Epithelial Intestinal HT-29 Cell Line." *The Annals of Occupational Hygiene* 56: 622–630. doi:10.1093/annhyg/mes005.

Smith, S., U. S. Cheng, and H. C. Yeh. 2001. "Deposition of Ultrafine Particles in Human Tracheobronchial Airways of Adults and Children." *Aerosol Science and Technology* 35: 697–709. doi:10.1080/02786820152546743.

Steinberg, P. 2016. "*In Vitro-In Vivo* Carcinogenicity." *Advances in Biochemical Engineering / Biotechnology* 157: 81–96. doi:10.1007/10_2015_5013.

Stratton, M. R., P. J. Campbell, and P. A. Futreal. 2009. "The Cancer Genome." *Nature* 458: 719–724. doi:10.1038/nature07943.

Sun, L., Y. Li, X. Liu, M. Jin, L. Zhang, Z. Du, C. Guo, et al. 2011. "Cytotoxicity and Mitochondrial Damage Caused by Silica Nanoparticles." *Toxicology In Vitro* 25: 1619–1629. doi:10.1016/j.tiv.2011.06.012.

Sutunkova, M. P., S. N. Solovyeva, B. A. Katsnelson, V. B. Gurvich, L. I. Privalova, I. A. Minigalieva, T. V. Slyshkina, et al. 2017. "A Paradoxical Response of the Rat Organism to Long-Term Inhalation of Silica-Containing Submicron (Predominantly Nanoscale) Particles of a Collected Industrial Aerosol at Realistic Exposure Levels." *Toxicology* 384: 59–68. doi:10.1016/j.tox.2017.04.010.

Sycheva, L. P., V. S. Zhurkov, V. V. Iurchenko, N. O. Daugel-Dauge, M. A. Kovalenko, E. K. Krivtsova, A. D. Durnev, et al. 2011. "Investigation of Genotoxic and Cytotoxic Effects of Micro- and Nanosized Titanium Dioxide in Six Organs of Mice *In Vivo*." *Mutation Research* 726: 8–14. doi:10.1016/j.mrgentox.2011.07.010.

Takagi, A., A. Hirose, T. Nishimura, N. Fukumori, A. Ogata, N. Ohashi, S. Kitajima, et al. 2008. "Induction of Mesothelioma in p53+/- Mouse by Intraperitoneal Application of Multi-Wall Carbon Nanotube." *The Journal of Toxicological Sciences* 33: 105–116. doi:10.2131/jts.33.105.

Talebi, A. R., L. Khorsandi, and M. Moridian. 2013. "The Effect of Zinc Oxide Nanoparticles on Mouse Spermatogenesis." *Journal of Assisted Reproduction and Genetics* 30: 1203–1209. doi:10.1007/s10815-013-0078-y.

Tarantini, A., R. Lanceleur, A. Mourot, M.-T. Lavault, G. Casterou, G. Jarry, K. Hogeveen, et al. 2015. "Toxicity, Genotoxicity and Proinflammatory Effects of Amorphous Nanosilica in the Human Intestinal Caco-2 Cell Line." *Toxicology In Vitro: An International Journal Published in Association with Bibra* 29: 398–407. doi:10.1016/j.tiv.2014.10.023.

Trachootham, D., J. Alexandre, and P. Huang. 2009. "Targeting Cancer Cells by ROS-Mediated Mechanisms: A Radical Therapeutic Approach?" *Nature Reviews Drug Discovery* 8: 579–591. doi:10.1038/nrd2803.

Uboldi, C., G. Giudetti, F. Broggi, D. Gilliland, J. Ponti, and F. Rossi. 2012. "Amorphous Silica Nanoparticles Do Not Induce Cytotoxicity, Cell Transformation or Genotoxicity in Balb/3T3 Mouse Fibroblasts." *Mutation Research* 745: 11–20. doi:10.1016/j.mrgentox.2011.10.010.

Vales, G., L. Rubio, and R. Marcos. 2015. "Long-Term Exposures to Low Doses of Titanium Dioxide Nanoparticles Induce Cell Transformation, But Not Genotoxic Damage in BEAS-2B Cells." *Nanotoxicology* 9: 568–578. doi:10.3109/17435390.2014.957252.

Vasseur, P., and C. Lasne. 2012. "OECD Detailed Review Paper (DRP) Number 31 on 'Cell Transformation Assays for Detection of Chemical Carcinogens': Main Results and Conclusions" *Mutation Research* 744: 8–11. doi:10.1016/j.mrgentox.2011.11.007.

Vogelstein, B., N. Papadopoulos, V. E. Velculescu, S. Zhou, L. A. Diaz, Jr., and K. W. Kinzler. 2013. "Cancer Genome Landscapes." *Science (New York, NY)* 339: 1546–1558. doi:10.1126/science.1235122.

Vormer, T. L., F. Foijer, C. L. Wielders, and H. Te Riele. 2008. "Anchorage-Independent Growth of Pocket Protein-Deficient Murine Fibroblasts Requires Bypass of G2 Arrest and can be Accomplished by Expression of TBX2." *Molecular and Cellular Biology* 28: 7263–7273. doi:10.1128/MCB.00313-08.

Wang, L., S. Luanpitpong, V. Castranova, W. Tse, Y. Lu, V. Pongrakhananon, Y. Rojanasakul, et al. 2011. "Carbon Nanotubes Induce Malignant Transformation and Tumorigenesis of Human Lung Epithelial Cells." *Nano Letters* 11: 2796–2803. doi:10.1021/nl2011214.

Wang, W., Y. Li, X. M. Liu, M. H. Jin, H. Y. Du, Y. Liu, P. Huang, et al. 2013. "Multinucleation and Cell Dysfunction Induced by Amorphous Silica Nanoparticles in an L-02 Human Hepatic Cell Line." *International Journal of Nanomedicine* 8: 3533–3541. doi:10.2147/IJN.S46732.

Wang, Y., Z. Zhang, H. Wang, Y. Zhang, M. Ji, H. Xu, C. Wang, et al. 2016. "miR-138-1* Regulates Aflatoxin B1-Induced Malignant Transformation of BEAS-2B Cells by Targeting PDK1." *Archives of Toxicology* 90: 1239–1249. doi:10.1007/s00204-015-1551-4.

Yang, X., D. Wang, Y. Ma, X. Xu, Z. Zhu, X. Wang, H. Deng, et al. 2015. "Continuous Activation of Nrf2 and Its Target Antioxidant Enzymes Leads to Arsenite-Induced Malignant Transformation of Human Bronchial Epithelial Cells." *Toxicology and Applied Pharmacology* 289: 231–239. doi:10.1016/j.taap.2015.09.020.

Yao, Y., T. Chen, S. S. Shen, Y. Niu, T. L. DesMarais, R. Linn, E. Saunders, et al. 2015. "Malignant Human Cell Transformation of Marcellus Shale Gas Drilling Flow Back Water." *Toxicology and Applied Pharmacology* 288: 121–130. doi:10.1016/j.taap.2015.07.011.

Yu, Y., J. Duan, W. Geng, Q. Li, L. Jiang, Y. Li, Y. Yu, et al. 2015a. "Aberrant Cytokinesis and Cell Fusion Result in

Multinucleation in HepG2 Cells Exposed to Silica Nanoparticles." *Chemical Research in Toxicology* 28: 490–500. doi:10.1021/tx500473h.

Yu, Y., J. Duan, Y. Li, Y. Yu, M. Jin, C. Li, Y. Wang, et al. 2015b. "Combined Toxicity of Amorphous Silica Nanoparticles and Methylmercury to Human Lung Epithelial Cells." *Ecotoxicology and Environmental Safety* 112: 144–152. doi:10.1016/j.ecoenv.2014.10.026.

Yu, Y., J. Duan, Y. Yu, Y. Li, X. Liu, X. Zhou, K.-F. Ho, et al. 2014. "Silica Nanoparticles Induce Autophagy and Autophagic Cell Death in HepG2 Cells Triggered by Reactive Oxygen Species." *Journal of Hazardous Materials* 270: 176–186. doi:10.1016/j.jhazmat.2014.01.028.

Zhang, Z., C. Kleinstreuer, and C. S. Kim. 2008. "Airflow and Nanoparticle Deposition in a 16-Generation Tracheobronchial Airway Model." *Annals of Biomedical Engineering* 36: 2095–2110. doi:10.1007/s10439-008-9583-z.

Zhang, Z., H. Lu, F. Huan, C. Meghan, X. Yang, Y. Wang, X. Wang, et al. 2014. "Cytochrome P450 2A13 Mediates the Neoplastic Transformation of Human Bronchial Epithelial Cells at a Low Concentration of Aflatoxin B1." *International Journal of Cancer* 134: 1539–1548. doi:10.1002/ijc.28489.

Zhao, Y., Y. Xu, Y. Li, W. Xu, F. Luo, B. Wang, Y. Pang, et al. 2013. "NF-κB-Mediated Inflammation Leading to EMT via miR-200c is Involved in Cell Transformation Induced by Cigarette Smoke Extract." *Toxicological Sciences: An Official Journal of the Society of Toxicology* 135: 265–276. doi:10.1093/toxsci/kft150.

Zou, Y., Q. Li, L. Jiang, C. Guo, Y. Li, Y. Yu, Y. Li, et al. 2016. "DNA Hypermethylation of CREB3L1 and Bcl-2 Associated with the Mitochondrial-Mediated Apoptosis via PI3K/Akt Pathway in Human BEAS-2B Cells Exposure to Silica Nanoparticles." *PLoS One* 11: e0158475. doi:10.1371/journal.pone.0158475.